IEEE Access
Multidisciplinary | Rapid Review | Open Access Journal

Received March 21, 2019, accepted April 13, 2019, date of publication April 18, 2019, date of current version April 29, 2019.

Digital Object Identifier 10.1109/ACCESS.2019.2911965

A Broadband Shared-Aperture L/S/X-Band Dual-Polarized Antenna for SAR Applications

KE LI, TAO DONG, AND ZHENGHUAN XIA

State Key Laboratory of Space-Ground Integrated Information Technology, Beijing Institute of Satellite Information Engineering, Beijing 100095, China

Corresponding author: Tao Dong (dongtaoandy@163.com)

This work was supported in part by the Innovation Funds of Aerospace Science and Technology under Grant JSKFJ201604120007, and in part by the Innovation Funds of China Academy of Space Technology under Grant CAST2016021.

ABSTRACT This paper presents a novel tri-band antenna with dual polarizations and shared aperture. The proposed antenna operates at *L*-, *S*-, and *X*-bands with an approximate frequency ratio of 1:1.9:5.5. Three types of radiation elements resonating at different frequencies, including the square microstrip patch, microstrip dipole, and printed monopole, are interlaced in the same aperture. Printed monopole with a fork-shaped stub is adopted as the *L*-band element due to its wideband ability. Both the *S*- and *X*-band elements adopt a stacked structure to enhance the bandwidth. Besides, the *S*-band element employs a stepped gradient structure that can obtain a wider bandwidth than the normal microstrip dipole. The measured results agree well with the simulations. The measured impedance bandwidths of *L*-, *S*-, and *X*-bands are 21.7%, 11.6%, and 18.9%, respectively. The measured isolation at *L*-, *S*-, and *X*-bands is higher than 25, 38, and 29 dB, respectively. The antenna also exhibits an excellent radiation performance with the high cross-polarization discrimination at the three bands. To the best of the authors' knowledge, this is the first shared-aperture *L*-/*S*-/*X*-band dual-polarized broadband antenna in a true sense, which is useful for potential synthetic aperture radar applications.

INDEX TERMS Antenna array, broadband, shared-aperture, L/S/X-band, dual-polarized, synthetic aperture radar (SAR).

I. INTRODUCTION

As a multipurpose sensor, synthetic aperture radar (SAR) can be applied in observation and imaging in any weather conditions and throughout the day and night [1]. It is widely used in various fields, such as natural resources monitoring, emergency control, and marine surveillance. Compared with the single-band and single-polarized SAR, the multi-band and multi-polarized SAR can obtain more electromagnetic scattering information to improve the ability of detection and resolution. And thus, it has become a popular trend in the area of spaceborne and airborne SAR [2].

However, the introduction of multi-band and multi-polarization means greater load weight and volume for spaceborne and airborne SAR. Shared-aperture antenna, which combines multiple antennas with different frequencies and polarization characteristics in the same aperture through reasonable design, can effectively reduce the overall volume and weight while guaranteeing the performance of each antenna [3]–[6]. Therefore, the multi-band and multi-polarized antenna with shared aperture has attracted a lot of research interests [7]–[9].

In recent years, various shared-aperture antennas with different radiation elements have been reported [10]–[19]. In [14], square patches and square perforated patches are interlaced for C- and L-band operations. In [15], circular patches and modified circular patches are interlaced to share the same aperture operating at C- and X-bands. To date, the reported literatures still mainly focus on the dual-band dual-polarized antenna with small frequency ratio. Very a few works on the multi-band dual-polarized array with large frequency ratio have been reported. In [20], a tri-band dual-polarized antenna is presented, showing the operation bands at X-, Ku-, and Ka-bands, but the impedance bandwidths of three bands are only 3.6%, 6.7%, and 5.3%, respectively. In [21], a tri-band dual-polarized antenna operating at L-, S-, and X-bands is presented, but the antenna is composed of a L/S sub-array and a L/X sub- array. It does not truly realize the shared aperture of three bands.

There are several challenges in the design of dual-band dual-polarized antenna due to both the constraints of radiation elements and the difficulty in implementing feed networks for

The associate editor coordinating the review of this manuscript and approving it for publication was Sotirios Goudos.

each band. This becomes more challenging if dual polarizations are required as the third band is introduced. Moreover, for the large frequency ratio operations, the element spacing of different antenna arrays must be reasonably designed to avoid the grating lobes. In addition, the impedance bandwidth of the low-frequency band is still narrow according to the reported literatures. In order to obtain higher range resolution in the SAR system, the bandwidth of the low-frequency band should be further broadened.

In order to solve the above problems, a novel tri-band dual-polarized shared-aperture antenna is proposed in this paper. The antenna operates at L-, S- and X-bands with different radiation elements, including square microstrip patch, microstrip dipole and printed monopole. The selection of these elements makes the most of the aperture. Due to the big difference of the element structures and the large frequency ratio, the interaction among the three frequency bands is small. In addition, the tri-band dual-polarized feed networks are placed on different planes, so the channel interferences among the three frequency bands can be reduced.

Compared with the reported works, the advantages of the proposed antenna can be summarized as follows:

1) The proposed antenna has a large frequency ratio of 1:1.9:5.5. To the best of the authors' knowledge, this work is the first real L/S/X-band dual-polarized antenna for SAR applications. For the proposed antenna, the elements of three bands are placed in a shared aperture.

2) The measured impedance bandwidths of the proposed antenna for L-, S- and X-bands, reach up to 21.7%, 11.6%, and 18.9%, respectively. And the measured impedance bandwidths are wider than that of most of the referenced designs.

II. ANTENNA CONFIGURATION

A. SPECIFICATIONS

The proposed antenna is designed for SAR applications. The specifications of the tri-band dual-polarized antenna are listed in TABLE 1. The central frequencies for L-, S, and X-band operations are designed as 1.75 GHz, 3.27 GHz, and 9.55 GHz, respectively. The frequency ratio is approximately 1:1.9:5.5. The impedance bandwidth for the X-band is about 1.8 GHz, and the impedance bandwidths for the L- and S-band are 230 MHz and 380 MHz, respectively. Dual polarizations are required in all of the three operation bands.

TABLE 1. Specifications of the proposed antenna.

Parameters	L-band	S-band	X-band
Center Frequency (GHz)	1.75	3.27	9.55
Bandwidth (MHz)	230	380	1800
Polarization	Dual-polarized	Dual-polarized	Dual-polarized
Isolation (dB)	22	38	29

B. CONFIGURATION

Fig. 1 shows the configuration of the proposed L/S/X-band dual-polarized antenna with a shared aperture. The proposed antenna contains a 6×6 X-band array, a 2×2 S-band array, and two separated L-band elements. Usually, the low-frequency radiation elements are placed on the bottom layer, while the high-frequency radiation elements are placed on the top layer due to its small size of structure. However, a novel scheme is adopted in this paper, as shown in Fig. 2. From the lowest layer to the top, the radiation elements from the highest frequency to the lowest frequency are placed in turn. By this way, the L-band elements can be easily interlaced with the S/X-band elements and the bandwidth of the low-frequency band can be improved effectively.

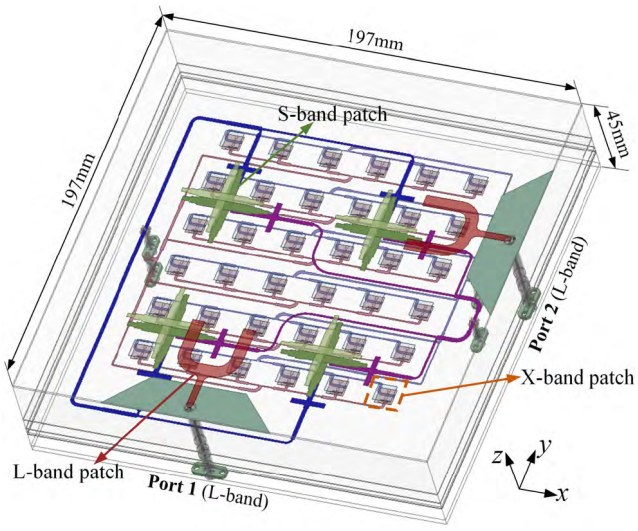

FIGURE 1. Configuration of the proposed shared-aperture L/S/X-band dual-polarized antenna.

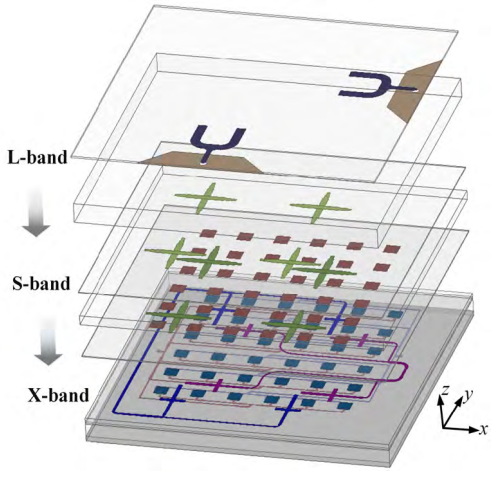

FIGURE 2. Exploded view of the proposed antenna.

To share the same aperture, different radiation elements including square microstrip patch, microstrip dipole and printed monopole are employed. For the X-band operation, the square patches are utilized and fed by the slot coupling.

For the S-band operation, the microstrip dipoles are adopted and fed by proximity coupling. In order to enhance the impedance bandwidth and gain, both X- and S-band

antennas employ the parasitic patches. Moreover, the printed monopole fed by microstrip line is selected as the L-band element and placed on the top layer of the whole structure.

Details of the proposed antenna design are given and discussed as below. The High Frequency Structure Simulator (HFSS) is employed in the optimization process to obtain the optimized structural parameters.

C. X-BAND ELEMENT

Fig. 3 shows the configuration of the X-band dual-polarized antenna element. The antenna has a stacked structure, which includes three substrates and two foam spacers. Rogers 5880 substrates with a permittivity of 2.2 and loss tangent of 0.0009 are used for the boards S1, S2 and S4. Foam spacers with a permittivity of 1.06 are used for the boards S0 and S3. The driven patch is printed on the top layer of the substrate S2 and fed through slot coupling by two perpendicular microstrip lines on the bottom layer to achieve the dual polarizations. The H-shaped slots are used for reducing the length of the slot while improving the isolation. The slots on the ground plane are placed as T-shaped for enhancing the isolation between the two ports. To improve the impedance bandwidth of the X-band operation, a parasitic patch is placed on the bottom of the substrate S4.

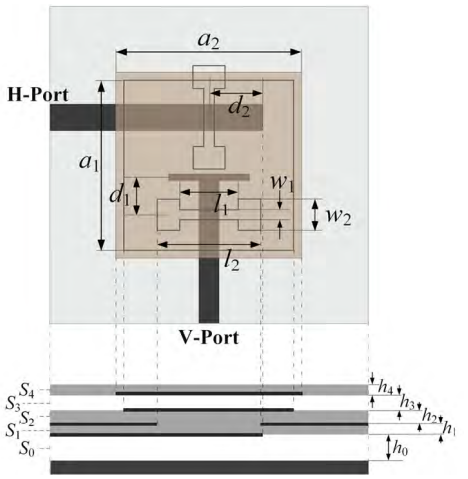

FIGURE 3. Configuration of the X-band radiation element.

The resonant frequencies of the driven patch f_{01} and parasitic patch f_{02} can be represented as below [20].

$$f_{01} = \frac{c}{2a_1\sqrt{\varepsilon_{c1}}} \text{ and } f_{02} = \frac{c}{2a_2\sqrt{\varepsilon_{c2}}} \quad (1)$$

where c is the speed of light in free space, ε_{c1} and ε_{c2} are the effective dielectric constants of lower substrate and upper substrate respectively, a_1 and a_2 are the lengths of the driven patch and parasitic patch respectively. Using equation (1), the resonant frequencies can be controlled independently by tuning the lengths of the radiation patches. The height (h_3) of the foam spacer S3 between S2 and S4 also has an important influence on the resonant frequencies. The X-band operation frequency is designed as 9.55 GHz. The wideband impedance matching can be achieved by adjusting the size of the slots and feed lines appropriately. The antenna is optimized using the simulation software and the optimized parameters are given in TABLE 2.

TABLE 2. Parameters of the X-band antenna: (mm).

a_1	a_2	h_0	h_1	h_2	h_3	h_4	d_1
7.95	8.62	7.7	0.5	1.0	2.3	0.5	1.2
d_2	l_1	w_1	l_2	w_2			
3.02	3.0	0.6	5.54	1.1			

D. S-BAND ELEMENT

In order to share the aperture with the X-band antenna, the strip-shaped microstrip dipole is employed as the S-band element. Fig. 4 shows the exploded view of the S/X-band antenna. The microstrip dipole is embedded in the middle of the X-band patches and fed by proximity coupling, which has less effect on the X-band radiation. The S-band antenna element also employs a stacked structure to enhance the bandwidth, as shown in Fig. 5. Most of its radiation structures and feeding structures share the same layer of substrate with the X-band elements. The S-band dual-polarized radiation patches are printed on the top and bottom layers of the substrate S4, respectively. The S-band parasitic patches are printed on both sides of the Rogers 5880 substrate S6. The feed lines which employ microstrip tuning branches to enhance the bandwidth are printed on the top layer of the substrate S2.

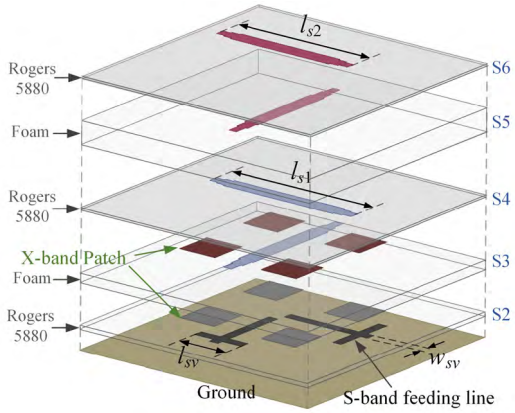

FIGURE 4. Exploded view of the S/X-band antenna.

The length of the dipole is about a half wavelength of the operation frequency of 3.27 GHz. The width of the microstrip dipole has an important influence on the impedance bandwidth. For the microstrip dipole, the bigger width of dipole relates to the wider impedance bandwidth. However, too bigger width of dipole will lead to strong coupling between S-band dipole and X-band parasitic patch, which will make the antenna performance worse. To achieve wider bandwidth, a stepped gradient patch is applied in the S-element as

shown in Fig. 5. Compared with the conventional microstrip dipole with a rectangular structure [21], the proposed S-band antenna has wider impedance bandwidth. In addition, the symmetrical structure can improve the cross-polarization characteristics of the antenna. Through the simulation, the optimized parameters can be obtained as shown in TABLE 3.

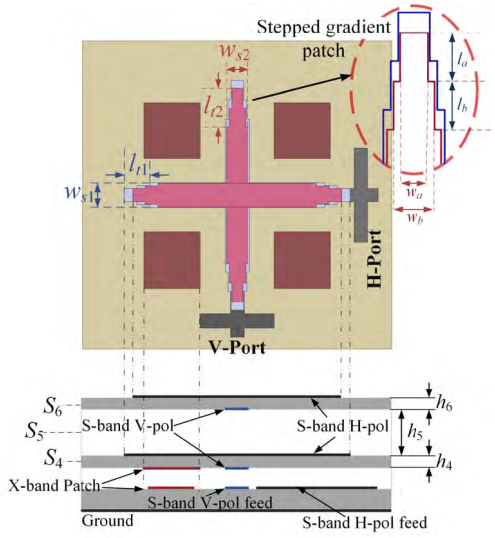

FIGURE 5. Configuration of the S-band radiation element.

TABLE 3. Parameters of the S-band antenna: (mm).

h_5	h_6	l_{s1}	l_{s2}	w_{s1}	w_{s2}	w_{sv}
5.7	0.5	40.9	38.6	4.38	3.83	2.38
l_{sv}	l_{t1}	l_{t2}	w_a	l_a	w_b	l_b
16.0	7.42	7.42	1.96	3.71	2.90	3.71

E. L-BAND ELEMENT

The configuration of the L-band radiation element is shown in Fig. 6. A monopole antenna with a fork-shaped stub is employed as the L-band element due to its merit of wide bandwidth. The monopole is printed on the top side of the FR4 substrate S8 with a permittivity of 4.4 and loss tangent of 0.02, while the trapeziform ground is printed on the bottom side of the substrate S8. The fork-shaped stub is arranged in the middle of the gap of the X-band patches to minimize the interference. L- and S-band antennas are separated by the foam spacer S7. Dual polarizations can be achieved by placing two elements vertically with each other. The monopole is fed by a 50-Ω microstrip line, which connects with a vertical soldered SMA connector.

The width (w_p) of the fork-shaped stub and the length (l_{p1}) of the horizontal section have an important influence on the impedance matching. The bigger w_p and l_{p1} will lead to lower resonant frequency, but the gap of X-band patches limits the size of the fork-shaped tuning stub. Considering the arrangement of the aperture and the size of antenna,

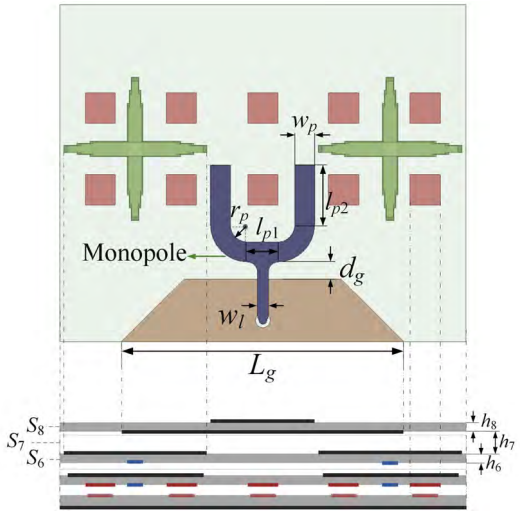

FIGURE 6. Configuration of the L-band radiation element.

the L- band operation frequency is set as 1.75 GHz. The optimized parameters of the L-band element are listed in TABLE 4.

TABLE 4. Parameters of the L-band antenna: (mm).

L_g	d_g	w_l	l_{p1}	l_{p2}	w_p	r_p
80.8	5.0	3.03	8.7	17.1	5.62	4.9

In addition, the X-band ground reflects the L-band microwave to obtain the unidirectional radiation. To obtain good impedance matching and radiation performance, the distance between the L-band element and the reflector should be a quarter of wavelength (λ_L) of the L-band center frequency. Considering reducing the profile, the distance between the L-band element and the reflector is finally optimized as 34 mm by the simulation, which is $0.18\lambda_L$. The height (h_7) of the foam spacer is 23 mm.

The proposed L-band element can obtain a wider bandwidth compared with the conventional shared-aperture antenna which usually uses a narrow slot or dipole as the low-frequency radiation element. Moreover, the proposed L-band antenna has less influence on the other bands due to its different style, compact structure, and independent ground.

III. FEED NETWORKS

Accommodating the feed networks of different polarizations and operation bands in a compact aperture is a major challenge in the design of shared-aperture antenna. It is suggested that employing the higher-frequency feed network below the ground plane and the lower-frequency feed network above the ground plane. This is due to the fact that the higher-frequency feed produces higher spurious radiation [14], [16].

The proposed shared-aperture antenna consists of a 6×6 X-band array, a 2×2 S-band array, and two L-band elements. Owing to the different feeding methods in the X- and S-bands,

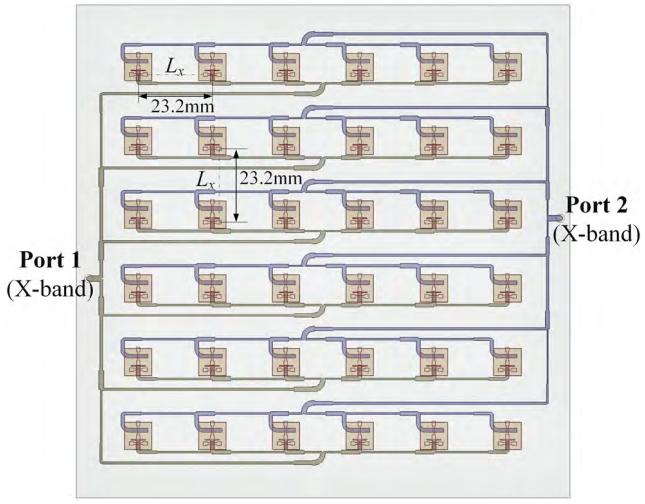

FIGURE 7. Layout of the X-band feed networks.

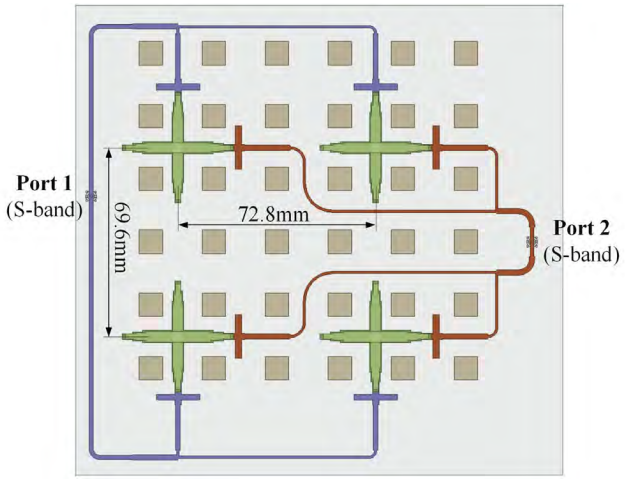

FIGURE 8. Layout of the S-band feed networks.

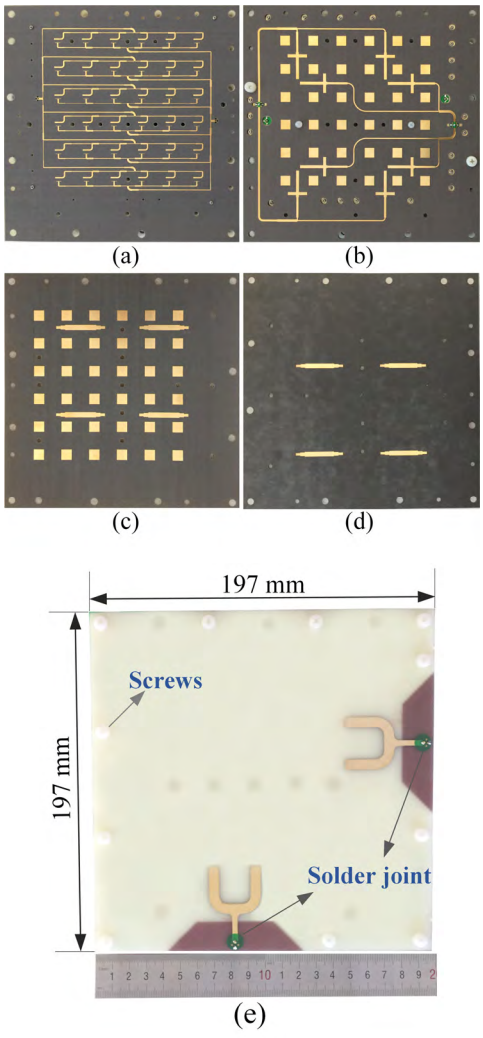

FIGURE 9. Prototype of the fabricated L/S/X-band dual-polarized antenna. (a) Layer S1 shows the X-band feed networks. (b) Layer S2 shows the X-band driven patches and S-band feed networks. (c) Layer S4 shows the X-band parasitic patches and S-band driven patches. (d) Layer S6 shows the S-band parasitic patches. (e) Top view of the assembled antenna.

it is feasible to print the X- and S-band feed networks on two sides of the ground plane, respectively.

A. X-BAND FEED NETWORKS

Fig. 7 shows the layout of the X-band feed networks. Parallel feed and series feed are combined in the X-band feed networks. Parallel feed guarantees the phase coincidence, while series feed can reduce the size of the feed networks.

To guarantee the consistent phase characteristics among the elements, the spacing between two adjacent elements should be one guided wavelength of X-band operation frequency. It can be expressed as follows:

$$L_x = L_y \approx \frac{c}{f_c\sqrt{\varepsilon_{eff}}} \tag{2}$$

where ε_{eff} is the effective dielectric constant of substrate S1 and f_c is the center frequency of the operation band. The element spacing has an important effect on the radiation performance. Larger spacing leads to better radiation pattern at lower frequency, while smaller spacing leads to better radiation pattern at higher frequency. The element spacing is finally optimized as 23.2 mm. The designed feed networks have compact size, good phase coincidence, and good impedance matching over a wide bandwidth.

B. S-BAND FEED NETWORKS

Fig. 8 shows the layout of the S-band feed networks. The S-band feed networks share the same layer with the X-band driven patch. The techniques of reverse-phase feed and series feed are employed to improve the polarization purity while maintaining a compact size [15]. To obtain a good radiation performance in the wide operation bandwidth, the horizontal and vertical distances between two adjacent elements are optimized as 72.8 mm and 69.6 mm, respectively. There is little overlap between the S- and X-band feed networks.

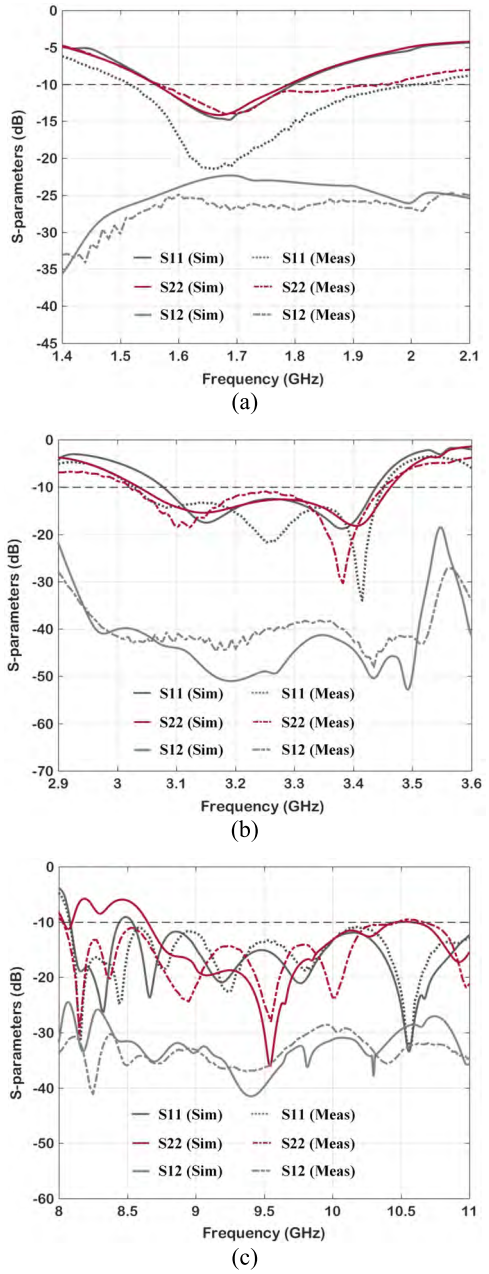

FIGURE 10. Simulated and measured S-parameters of the tri-band dual-polarized antenna. (a) L-band operation. (b) S-band operation. (c) X-band operation.

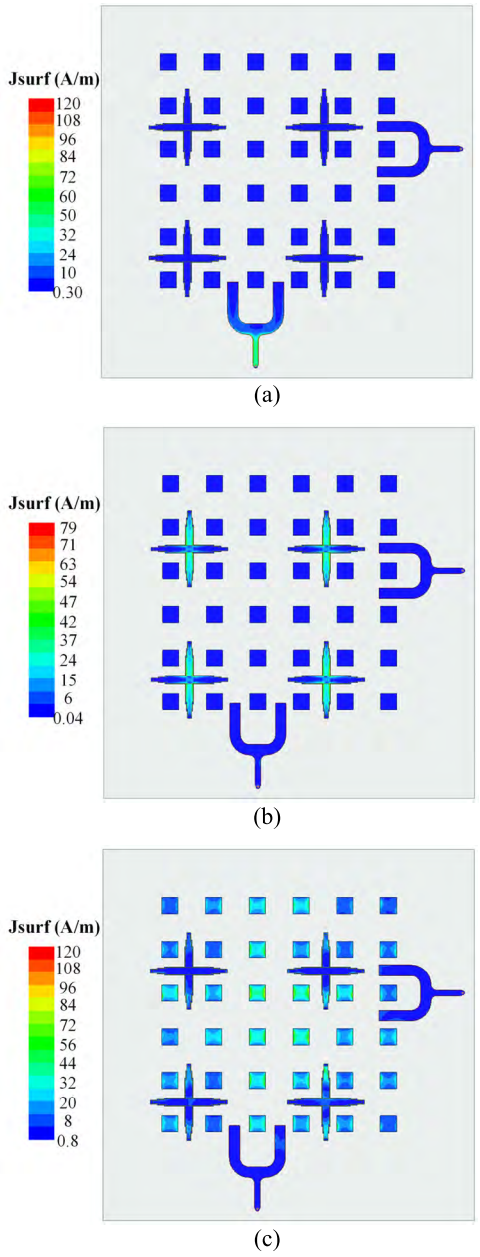

FIGURE 11. Current distribution of the proposed antenna. (a) 1.75 GHz, L band. (b) 3.27 GHz, S band. (c) 9.55 GHz, X band.

Moreover, the S- and X-band feed networks are printed on two sides of the ground. Thus the channel interferences between the two operation bands can be reduced.

IV. RESULTS AND DISCUSSION

To validate the simulation results, the proposed antenna is fabricated and the prototype is shown in Fig. 9. The S-parameters of the fabricated antenna are measured by a vector network analyzer and the results are shown in Fig. 10. It can be seen the measured results agree reasonably well with the simulation results.

For the L-band operation, a measured impedance bandwidth of 380 MHz ranging from 1.56 GHz to 1.94 GHz is achieved for the two polarizations as shown in Fig. 10(a). The measured bandwidth is slightly wider than the simulated one. The existence of the discrepancy between the measured and simulated results is mainly due to the effect of SMA connector soldering and fabrication error. At the center frequency of 1.75 GHz, the reflection coefficients for the two polarizations are below −18 dB. The measured isolation between the two ports is over 25 dB.

For the S-band operation, the antenna achieves an impedance bandwidth of 380 MHz ranging from 3.08 GHz

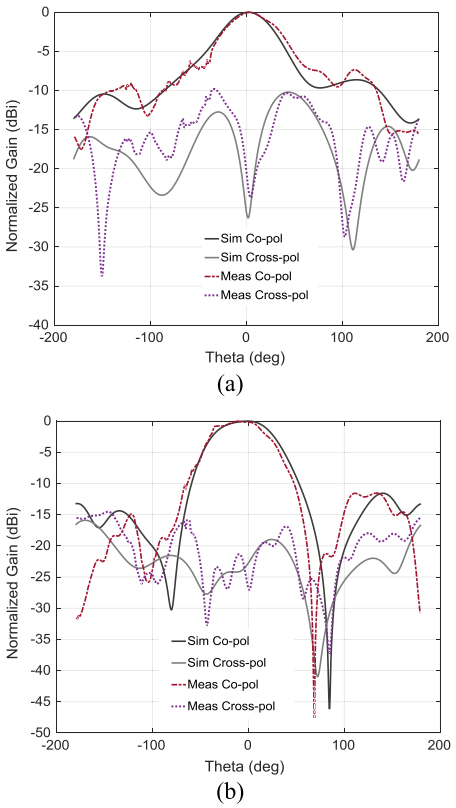

FIGURE 12. Simulated and measured radiation patterns of the proposed dual-polarized antenna at 1.9 GHz. (a) V-polarization. (b) H-polarization.

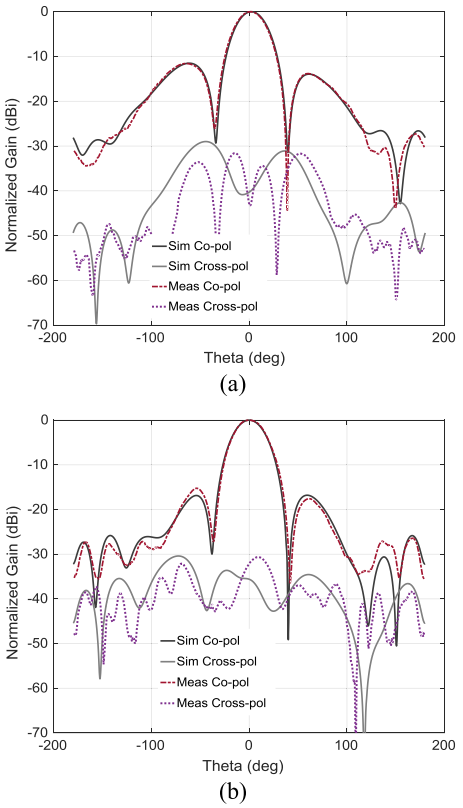

FIGURE 13. Simulated and measured radiation patterns of the proposed dual-polarized antenna at 3.25 GHz. (a) V-polarization. (b) H-polarization.

TABLE 5. Comparison with the reported designs.

Antennas	Operation bands	Impedance bandwidth	Frequency ratio
[16]	C, X	3.85%, 6.06%	1:1.92
[17]	C, X	7.94%, 6.25%	1:1.81
[18]	S, C	15.6%, 9.30%	1:2.09
[19]	X, Ku	8.30%, 18.9%	1:1.44
[20]	X, Ku, Ka	3.6%, 6.7%, 5.2%	1:1.54:3.59
This work	L, S, X	21.7%, 11.6%, 18.9%	1:1.9:5.5

to 3.46 GHz as shown in Fig. 10(b). The isolation between the two ports is over 38 dB in the operation band.

In the X-band, a wide impedance bandwidth of 1.8 GHz ranging from 8.65 GHz to 10.45 GHz is achieved as shown in Fig. 10(c). The isolation between the two ports is over 29 dB in the operation band.

The fractional impedance bandwidths at L-, S-, and X-bands can be calculated to be 21.7%, 11.6%, and 18.9%, respectively. TABLE 5 compares the proposed shared- aperture tri-band dual-polarized antenna with other reported designs in [16]–[20]. The comparison focuses on the impedance bandwidth and frequency ratio. This comparison demonstrates that the proposed antenna has a larger frequency ratio and wider impedance bandwidth than the reported designs in [16]–[20].

To better understand the antenna behavior, the simulated current patterns of the proposed antenna are given in Fig. 11. In Fig. 11(a), it's observed that there is very few current on the S- and X- band elements when antenna operates at L-band excited by Port 1. This is because the L-band radiation elements are placed on the top layer and far from the elements of other bands. When the antenna operates at S-band, the current mainly flows on the microstrip dipole as shown in Fig. 11(b). In Fig. 11(c), there is a strong current distribution on the square patches when the antenna operates at X-band. In contrast, the current on the S- and L-band elements are much weaker. Conclusion can be made that there is little interference among the three bands.

The radiation performance of the proposed antenna in the three operation bands is also measured and the results are shown in Figs. 12-14. The simulated and measured radiation patterns of the L-band dual-polarized antenna at 1.9 GHz are normalized and shown in Fig. 12. It can be seen that the measured results agree well with the simulation results. The measured cross-polarization discriminations (XPDs) in the broadside direction are higher than 20 dB for the two polarizations.

The normalized radiation patterns of the 2×2 S-band dual-polarized array at 3.25 GHz are shown in Fig. 13. It's observed that the measured XPDs are higher than 30 dB in the broadside direction. The side lobes are measured to be lower than −11.5 dB and −15 dB for the V- and H-polarization, respectively.

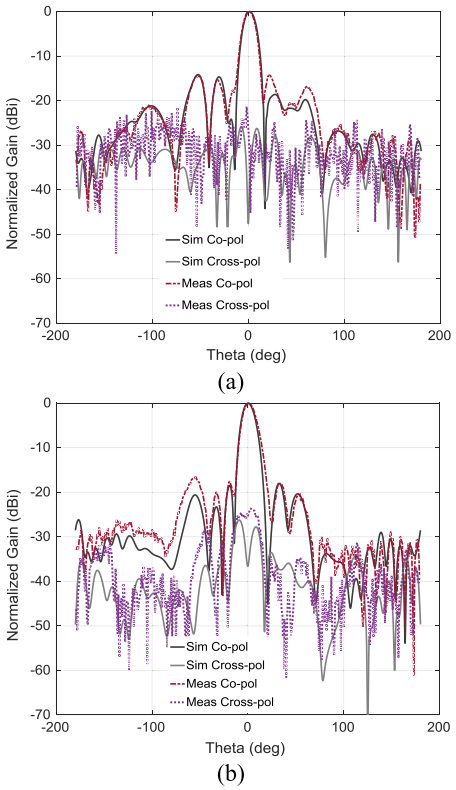

FIGURE 14. Simulated and measured radiation patterns of the proposed dual-polarized antenna at 9.5 GHz. (a) V-polarization. (b) H-polarization.

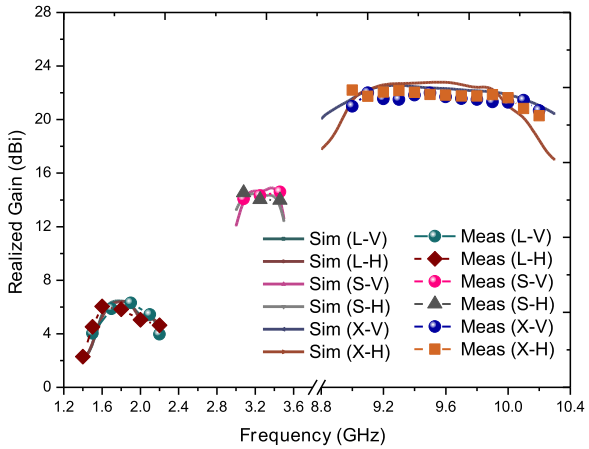

FIGURE 15. Simulated and measured realized gain of the proposed L/S/X-band dual-polarized antenna.

Fig. 14 shows the simulated and measured normalized radiation patterns of the 6×6 X-band dual-polarized array at 9.5 GHz. The measured XPDs are higher than 22 dB in the broadside direction. The measured side lobes are lower than −14.5 dB and −16.5 dB for the V- and H-polarization, respectively.

Fig. 15 shows the simulated and measured realized gain of the proposed tri-band antenna. It is observed that the measured and simulated gains agree well with each other. When the L-band antenna is excited, the antenna exhibits a gain of over 5 dBi ranging from 1.56 GHz to 1.94 GHz. At the frequency of 1.9 GHz, the measured gain of V-polarization is higher than 6.3 dBi. For the S-band operation, the two polarizations achieve the gains higher than 14 dBi ranging from 3.08 GHz to 3.46 GHz. When the X-band array is excited, the antenna exhibits a fat gain of 21 dBi for both of the two polarizations ranging from 9 GHz to 10 GHz. The minor discrepancy between the simulated and measured results occurs at the X band, which is mainly attributed to the errors in the process of assembling multiple substrates.

V. CONCLUSION

In this paper, a tri-band dual-polarized shared-aperture antenna operating at L-, S- and X-bands for SAR applications is presented. Three kinds of radiation elements, including square microstrip patch, microstrip dipole and printed monopole, are employed as the elements of three operation bands. Different from the conventional shared-aperture antenna, the low-frequency element is placed on the top layer to achieve wider bandwidth at the low-frequency band. To accommodate the feed networks within a compact area, multiple feeding methods are combined, such as parallel feed and series feed. The feed networks of three operation bands are placed on different planes, thus the channel interferences among the three operation bands can be reduced. The proposed antenna is optimized, fabricated and tested, showing an impedance bandwidth of 21.7%, 11.6%, and 18.9% at L-, S-, and X-bands, respectively. The measured isolation at L-, S- and X-bands, is over 25 dB, 38 dB and 29 dB, respectively. The antenna also exhibits good radiation performance in each operation band. The proposed antenna achieves a wide bandwidth in all of the three operation bands with a compact size. It is suitable for the future SAR applications.

ACKNOWLEDGMENT

The authors would like to thank Dr. Zhihui Liu and Dr. Jingwen He for their supports in review and discussions.

REFERENCES

[1] V. Ravindra, P. R. Akbar, M. Zhang, J. Hirokawa, H. Saito, and A. Oyama, "A dual-polarization *X*-band traveling-wave antenna panel for small-satellite synthetic aperture radar," *IEEE Trans. Antennas Propag.*, vol. 65, no. 5, pp. 2144–2156, May 2017.

[2] C.-X. Mao *et al.*, "X/Ka-band dual-polarized digital beamforming synthetic aperture radar," *IEEE Trans. Microw. Theory Techn.*, vol. 65, no. 11, pp. 4400–4407, Nov. 2017.

[3] R. Y. Deng, S. H. Xu, F. Yang, and M. K. Li, "An FSS-backed Ku/Ka quad-band reflectarray antenna for satellite communications," *IEEE Trans. Antennas Propag.*, vol. 66, no. 8, pp. 4353–4358, Aug. 2018.

[4] W. Li *et al.*, "Design of a dual-band dual-polarization transparent frequency selective surface," *IEEE Antennas Wireless Propag. Lett.*, vol. 16, pp. 3172–3175, 2017.

[5] L. L. Shafai, W. A. Chamma, M. Barakat, P. C. Strickland, and G. Seguin, "Dual-band dual-polarized perforated microstrip antennas for SAR applications," *IEEE Trans. Antennas Propag.*, vol. 48, no. 1, pp. 58–66, Jan. 2000.

[6] M. M. Honari, R. Mirzavand, H. Saghlatoon, and P. Mousavi, "A dual-band low-profile aperture antenna with substrate-integrated waveguide grooves," *IEEE Trans. Antennas Propag.*, vol. 64, no. 4, pp. 1561–1566, Apr. 2016.

[7] X. Qu, S. S. Zhong, Y. M. Zhang, and W. Wang, "Design of an S/X dual-band dual-polarised microstrip antenna array for SAR applications," *IET Microw., Antennas Propag.*, vol. 1, no. 2, pp. 513–517, Apr. 2007.
[8] Y. Chen and R. G. Vaughan, "Dual-polarized *L*-band and single-polarized *X*-band shared-aperture SAR array," *IEEE Trans. Antennas Propag.*, vol. 66, no. 7, pp. 3391–3400, Jul. 2018.
[9] L. Kong and X. Xu, "A compact dual-band dual-polarized microstrip antenna array for MIMO-SAR applications," *IEEE Trans. Antennas Propag.*, vol. 66, no. 5, pp. 2374–2381, May 2018.
[10] A. Boukarkar, X. Q. Lin, Y. Jiang, L. Y. Nie, P. Mei, and Y. Yu, "A miniaturized extremely close-spaced four-element dual-band MIMO antenna system with polarization and pattern diversity," *IEEE Antennas Wireless Propag. Lett.*, vol. 17, no. 1, pp. 134–137, Jan. 2018.
[11] S. H. Yeung, A. García-Lampérez, T. K. Sarkar, and M. Salazar-Palma, "Thin and compact dual-band four-element broadside patch antenna arrays," *IEEE Antennas Wireless Propag. Lett.*, vol. 13, no. , pp. 567–570, 2014.
[12] S. E. Valavan, D. Tran, A. G. Yarovoy, and A. G. Roederer, "Dual-band wide-angle scanning planar phased array in X/Ku-bands," *IEEE Trans. Antennas Propag.*, vol. 62, no. 5, pp. 2514–2521, May 2014.
[13] D. M. Pozar and S. D. Targonski, "A shared-aperture dual-band dual-polarized microstrip array," *IEEE Trans. Antennas Propag.*, vol. 49, no. 2, pp. 150–157, Feb. 2001.
[14] G. Vetharatnam, C. B. Kuan, and C. H. Teik, "Combined feed network for a shared-aperture dual-band dual-polarized array," *IEEE Antennas Wireless Propag. Lett.*, vol. 4, pp. 297–299, 2005.
[15] C.-X. Mao, S. Gao, Y. Wang, Q.-X. Chu, and X.-X. Yang, "Dual-band circularly polarized shared-aperture array for *C*-/*X*-band satellite communications," *IEEE Trans. Antennas Propag.*, vol. 65, no. 10, pp. 5171–5178, Oct. 2017.
[16] C.-X. Mao, S. Gao, Y. Wang, Q. Luo, and Q.-X. Chu, "A shared-aperture dual-band dual-polarized filtering-antenna-array with improved frequency response," *IEEE Trans. Antennas Propag.*, vol. 65, no. 4, pp. 1836–1844, Apr. 2017.
[17] F. Qin *et al.*, "A simple low-cost shared-aperture dual-band dual-polarized high-gain antenna for synthetic aperture radars," *IEEE Trans. Antennas Propag.*, vol. 64, no. 7, pp. 2914–2922, Jul. 2016.
[18] H. Zhai, K. Zhang, S. Yang, and D. Feng, "A low-profile dual-band dual-polarized antenna with an AMC surface for WLAN applications," *IEEE Antennas Wireless Propag. Lett.*, vol. 16, pp. 2692–2695, 2017.
[19] J.-D. Zhang, W. Wu, and D.-G. Fang, "Dual-band and dual-circularly polarized shared-aperture array antennas with single-layer substrate," *IEEE Trans. Antennas Propag.*, vol. 64, no. 1, pp. 109–116, Jan. 2016.
[20] C.-X. Mao, S. Gao, Q. Luo, T. Rommel, and Q.-X. Chu, "Low-cost X/Ku/Ka-band dual-polarized array with shared aperture," *IEEE Trans. Antennas Propag.*, vol. 65, no. 7, pp. 3520–3527, Jul. 2017.
[21] S.-S. Zhong, Z. Sun, L.-B. Kong, C. Gao, W. Wang, and M.-P. Jin, "Tri-band dual-polarization shared-aperture microstrip array for SAR applications," *IEEE Trans. Antennas Propag.*, vol. 60, no. 9, pp. 4157–4165, Sep. 2012.

KE LI was born in Meishan, China. He received the B.S. degree in electronic information science and technology from the University of Electronic Science and Technology, in 2011, and the Ph.D. degree in physical electronics from the Institute of Electronics, Chinese Academy of Sciences (CAS), in 2016. He is currently with the State Key Laboratory of Space-Ground Integrated Information Technology, Beijing Institute of Satellite Information Engineering. His research interests include ultra-wide band (UWB) antenna, dual-polarized antenna array, satellite antenna array, and multiband synthetic aperture radar antenna array.

TAO DONG received the B.S. and Ph.D. degrees in electronics science and technology from the Beijing Institute of Technology, in 1999 and 2004, respectively. He is currently a Professor with the State Key Laboratory of Space-Ground Integrated Information Technology, Beijing Institute of Satellite Information Engineering. His research interests include antenna, phased array, and opto-electronic devices.

ZHENGHUAN XIA received the Ph.D. degree in electromagnetic field and microwave technology from the Institute of Electronics, Chinese Academy of Sciences (CAS), in 2015. Since 2015, he has been with the State Key Laboratory of Space-Ground Integrated Information Technology, Beijing Institute of Satellite Information Engineering, where he became an Associate Professor, in 2017. His research interests include novel space-borne synthetic aperture radar (SAR) technology, ultra-wide band (UWB) radar systems, radar signal processing, and SAR imaging with FPGAs.